The Astrophysical Journal, 856:128 (13pp), 2018 April 1 https://doi.org/10.3847/1538-4357/aab610

Evidence for Pulsar-like Emission Components in the Broadband ULX Sample

D. J. Walton[1], F. Fürst[2], M. Heida[3], F. A. Harrison[3], D. Barret[4,5], D. Stern[6], M. Bachetti[7], M. Brightman[3], A. C. Fabian[1], and M. J. Middleton[8]
[1] Institute of Astronomy, University of Cambridge, Madingley Road, Cambridge CB3 0HA, UK
[2] European Space Astronomy Centre (ESA/ESAC), Operations Department, Villanueva de la Cañada (Madrid), Spain
[3] Space Radiation Laboratory, California Institute of Technology, Pasadena, CA 91125, USA
[4] Universite de Toulouse; UPS-OMP; IRAP; Toulouse, France
[5] CNRS; IRAP; 9 Av. colonel Roche, BP 44346, F-31028 Toulouse cedex 4, France
[6] Jet Propulsion Laboratory, California Institute of Technology, Pasadena, CA 91109, USA
[7] INAF/Osservatorio Astronomico di Cagliari, via della Scienza 5, I-09047 Selargius (CA), Italy
[8] Department of Physics and Astronomy, University of Southampton, Highfield, Southampton SO17 1BJ, UK
Received 2018 February 1; revised 2018 March 2; accepted 2018 March 8; published 2018 April 2

Abstract

We present broadband X-ray analyses of a sample of bright ultraluminous X-ray sources (ULX) with the goal of investigating the spectral similarity of this population to the known ULX pulsars, M82 X-2, NGC 7793 P13, and NGC 5907 ULX. We perform a phase-resolved analysis of the broadband *XMM-Newton*+*NuSTAR* data set of NGC 5907 ULX, finding that the pulsed emission from the accretion column in this source exhibits a similar spectral shape to that seen in both M82 X-2 and NGC 7793 P13, and that this is responsible for the excess emission observed at the highest energies when the spectra are fit with accretion disk models. We then demonstrate that similar "hard" excesses are seen in all ULXs in the broadband sample. Finally, for ULXs where the nature of the accretor is currently unknown, we test whether the hard excesses are all consistent with being produced by an accretion column similar to those present in M82 X-2, NGC 7793 P13, and NGC 5907 ULX. Based on the average shape of the pulsed emission, we find that in all cases a similar accretion column can successfully reproduce the observed data, consistent with the hypothesis that this ULX sample may be dominated by neutron star accretors. Compared to the known pulsar ULXs, our spectral fits for the remaining ULXs suggest that the non-pulsed emission from the accretion flow beyond the magnetosphere makes a stronger relative contribution than the component associated with the accretion column. If these sources do also contain neutron star accretors, this may help to explain the lack of detected pulsations.

Key words: stars: neutron – X-rays: binaries – X-rays: individual (NGC 5907 ULX)

1. Introduction

The discovery that three ultraluminous X-ray sources (ULX) are powered by accreting pulsars—M82 X-2: Bachetti et al. (2014), NGC 7793 P13: Fürst et al. (2016) and Israel et al. (2017b), and NGC 5907 ULX: Israel et al. (2017a)—has brought about a paradigm shift in our understanding of this exotic population. ULXs appear to radiate in excess of the Eddington limit for the standard $\sim 10\,M_{\odot}$ stellar remnant black holes seen in Galactic X-ray binaries (i.e., $L_{\rm X} > 10^{39}$ erg s^{-1}), and so black hole accretors had generally been assumed. The brightest ULXs were previously considered to be good candidates for intermediate-mass black holes ($10^2 \lesssim M_{\rm BH} \lesssim 10^5\ M_{\odot}$; Sutton et al. 2012) based on their extreme luminosities. However, the pulsar NGC 5907 ULX has an apparent peak X-ray luminosity of $\sim 7 \times 10^{40}$ erg s^{-1} (assuming isotropy; Fürst et al. 2017; Israel et al. 2017a), making it one of the brightest ULXs known (e.g., Swartz et al. 2004; Walton et al. 2011). These objects are therefore extreme, with luminosities up to $\sim$500 times the Eddington limit for a standard $1.4\,M_{\odot}$ neutron star ($\sim 2 \times 10^{38}$ erg s^{-1}).

Given that all three sources were known to be ULXs long before their identification as pulsars (e.g., Kaaret et al. 2009; Sutton et al. 2013a; Motch et al. 2014), it is natural to ask how many other members of the ULX population could also be powered by accretion onto a neutron star. Although pulsations have not currently been detected from any other members of the ULX population (Doroshenko et al. 2015), the pulsations in both M82 X-2 and NGC 5907 ULX are transient (Bachetti et al. 2014; Israel et al. 2017a). Exactly why this is the case is not currently well understood. Nevertheless, a lack of observed pulsations therefore does not exclude a neutron star accretor. King et al. (2017) suggest that even for ULXs that are powered by neutron stars, pulsations may only be observable when the magnetospheric radius is close to (or larger than) the spherization radius. The former is the point at which the accretion disk is truncated by the magnetic field of the neutron star, and the material is forced to follow the field lines instead, and the latter is the point at which the accretion disk transitions to the thick inner flow expected for super-Eddington accretion (e.g., Shakura & Sunyaev 1973; Abramowicz et al. 1988; Dotan & Shaviv 2011). This idea appears to be supported by our spectral analysis of NGC 7793 P13 (Walton et al. 2018).

Since it may not always be possible to identify neutron star ULXs through the detection of pulsations, and dynamical mass measurements are challenging owing to the faint stellar counterparts (e.g., Gladstone et al. 2013; Heida et al. 2014; López et al. 2017), other methods for identifying neutron star ULXs will be of key importance for our understanding of the nature of this population as a whole. Here, we investigate potential spectral signatures of neutron star ULXs by determining the properties of the pulsed emission from the three known systems, and assessing whether similar features are seen in the broader ULX population for which the nature of the accretors remains unknown. The paper is structured as follows: in Section 2 we perform a phase-resolved analysis of

the ULX pulsar NGC 5907 ULX for comparison with M82 X-2 and NGC 7793 P13, in Section 3 we compare the high-energy properties of the known ULX pulsars and the general ULX population, and in Section 4 we present fits to the broadband ULX sample with models directly motivated by the known ULX pulsars. We discuss our results in Section 5 and summarize our conclusions in Section 6.

2. The Pulsed Emission from NGC 5907 ULX

We begin by investigating the pulsed emission from NGC 5907 ULX in order to separate the emission from the accretion column (pulsed) from the rest of the accretion flow (assumed to be steady over the pulse cycle). For this analysis, we focus on the high-flux coordinated observation performed with the *NuSTAR* (Harrison et al. 2013) and *XMM-Newton* (Jansen et al. 2001) observatories in 2014 (a log of all the observations considered in this work is given in Appendix A), as this is the only broadband observation of NGC 5907 ULX in which the pulsations have been detected to date. We refer the reader to Fürst et al. (2017) for details on the reduction of these data, but note that here we are only able to utilize data from the EPIC-pn detector (Strüder et al. 2001) for the lower-energy *XMM-Newton* data, since the pulse period is shorter than the time resolution of the EPIC-MOS detectors.

2.1. Difference Spectroscopy

First, we isolate the spectrum of the pulsed component, similar to our recent analyses of M82 X-2 and NGC 7793 P13 (Brightman et al. 2016a; Walton et al. 2018). To do so, we follow the same approach as in those works and extract spectra from the brightest and the faintest quarters ($\Delta\phi_{\rm pulse} = 0.25$) of the pulse cycle (the pulse-profile of NGC 5907 ULX is nearly sinusoidal, similar to NGC 7793 P13 and M82 X-2; see Figure 1 in Israel et al. 2017a), and subtract the latter from the former (i.e.,"pulse-on"–"pulse-off"). Given the low signal-to-noise, we combine the data from the *NuSTAR* FPMA and FPMB detectors for NGC 5907 ULX throughout this work. The combined data are rebinned to have a minimum signal-to-noise ratio (S/N) per energy bin of 3 to ensure the errors are at least close to Gaussian and allow the use of χ^2 statistics. We fit the data over the ∼0.5–25 keV energy range with a simple CUTOFFPL model, allowing for neutral absorption from the Galactic column, fixed to $N_{\rm H,Gal} = 1.2 \times 10^{20}$ cm^{-2} (Kalberla et al. 2005), and intrinsic to NGC 5907 ($N_{\rm H,int}$; $z = 0.002225$) using the TBNEW absorption code. We adopt the abundances of Wilms et al. (2000) and the cross-sections of Verner et al. (1996) throughout this work. However, the intrinsic column is poorly constrained in these fits, so we fix it to 7×10^{21} cm^{-2} following previous analyses of the average broadband spectra (Walton et al. 2015a; Fürst et al. 2017).

As with both M82 X-2 and NGC 7793 P13, the simple CUTOFFPL model provides a good fit to the NGC 5907 ULX pulsed spectrum, with $\chi^2 = 24$ for 21 degrees of freedom (dof). Although the constraints are not as strong in this case, the results are also broadly similar to both M82 X-2 and NGC 7793 P13; the pulsed spectrum shows a hard rise before exhibiting a cutoff at fairly low energies: $\Gamma = 0.7^{+0.4}_{-0.5}$, $E_{\rm cut} = 5.5^{+4.8}_{-2.1}$ keV. We show the 2D confidence contours for Γ and $E_{\rm cut}$ in Figure 1 for all three of the pulsar ULXs currently known. While there are quantitative differences between them, all three sit in broadly the same area of parameter space in terms of their pulsed emission. For further comparison, the pulsed flux from NGC 5907 ULX during this epoch corresponds to an apparent 0.5–25.0 keV luminosity of $2.6^{+0.3}_{-0.4} \times 10^{40}$ erg s^{-1} (assuming isotropy) for a distance to NGC 5907 of 17.1 Mpc (Tully et al. 2016). This is significantly more luminous than the pulsed emission in both M82 X-2 and NGC 7793 P13, although this is not surprising given that NGC 5907 ULX is inferred to have a much higher phase-averaged luminosity than these other systems.

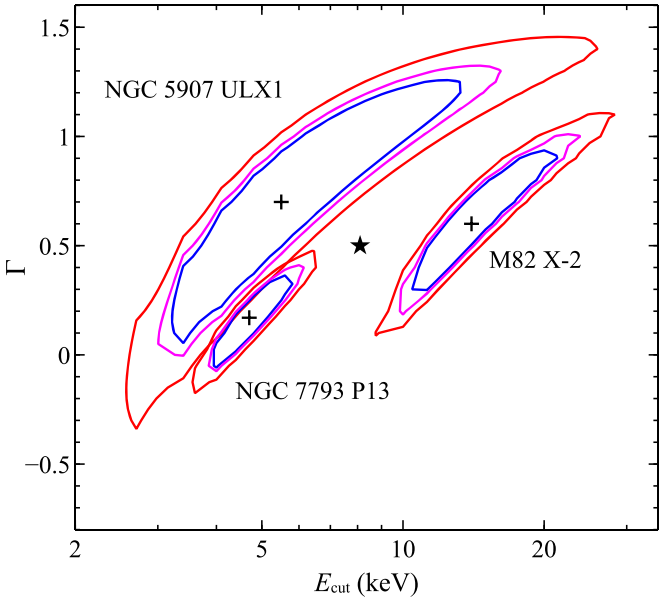

Figure 1. 2D confidence contours for Γ and $E_{\rm cut}$ for the pulsed spectra of M82 X-2, NGC 7793 P13, and NGC 5907 ULX1. The 90%, 95%, and 99% confidence contours for two parameters of interest are shown in blue, magenta, and red, respectively. The star shows the average of the best-fit values, which is utilized in our fits to the broadband ULX sample (Section 4).

2.2. Phase-resolved Spectroscopy

We also perform phase-resolved spectroscopy of NGC 5907 ULX, again following our analysis of NGC 7793 P13. We continue using phase bins of $\Delta\phi_{\rm pulse} = 0.25$ in size, and extract spectra from three different fluxes across the pulse cycle: high-flux (cycle peak), medium-flux (rise + fall), and low-flux (cycle minimum).[9] We fit the broadband spectra from all three phase bins simultaneously and undertake a simple decomposition of the data into stable (non-pulsed) and variable (pulsed) components. Based on our "pulse on"–"pulse-off" difference spectroscopy (Section 2.1), we treat the pulsed emission from the accretion column with a CUTOFFPL model. The "shape" parameters for this component (Γ, $E_{\rm cut}$) are linked across all three phase bins and are fixed to the results obtained above. The normalization of the CUTOFFPL component can vary between the phase bins, and we do not require this to be zero for the low-flux data, as the emission from the accretion column could still contribute during the minimum of the pulse cycle.

For the stable emission, which we expect to come from the accretion flow outside of $R_{\rm M}$, we initially fit a single DISKPBB component, following the time-averaged analyses in Walton

[9] As with NGC 7793 P13, we initially extracted the "rise" and "fall" spectra separately, but on inspection their spectra were found to be similar, and so were combined into a single medium-flux data set.

Table 1
Best-fit Parameters Obtained from Our Phase-resolved Analysis of the Broadband 2014 Observation of NGC 5907 ULX

Model Component	Parameter		Stable Continuum: DISKPBB	Stable Continuum: DISKBB+BB
TBABS	$N_{\rm H;int}$	[10^{21} cm^{-2}]	$6.7^{+0.7}_{-0.5}$	$7.5^{+1.4}_{-0.8}$
DISKPBB/DISKBB	$kT_{\rm in}$	[keV]	$2.8^{+0.5}_{-0.8}$	0.4 ± 0.1
	p		$0.57^{+0.04}_{-0.07}$	0.75 (fixed)
	Norm		$3.2^{+2.5}_{-1.9} \times 10^{-3}$	$0.8^{+3.4}_{-0.5}$
BB	kT	[keV]	...	1.2 ± 0.2
	Norm	[10^{-6}]	...	4.5 ± 1.3
CUTOFFPL	Γ		0.7[a]	
	$E_{\rm cut}$	[keV]	5.5[a]	
	F_{2-10}[b] (low)	[10^{-12} erg cm^{-2} s^{-1}]	<1.1	1.0 ± 0.1
	F_{2-10}[b] (med)	[10^{-12} erg cm^{-2} s^{-1}]	$1.1^{+0.3}_{-0.8}$	1.3 ± 0.1
	F_{2-10}[b] (high)	[10^{-12} erg cm^{-2} s^{-1}]	$1.3^{+0.4}_{-0.8}$	1.6 ± 0.1
χ^2/dof			383/385	370/384

Notes.
[a] These parameters have been fixed to the best-fit values from the "pulse on"–"pulse-off" difference spectroscopy (Section 2.1).
[b] Observed fluxes for the CUTOFFPL component in the 2–10 keV band.

et al. (2015a) and Fürst et al. (2017). This is a multi-color accretion disk model in which the radial temperature index of the disk (p) is free to vary in addition to its inner temperature ($T_{\rm in}$) and normalization. All the parameters for this component are linked across all three phase bins, as is the intrinsic neutral absorption column. The global fit to the phase-resolved data with this model is very good, χ^2/dof = 383/385, and the parameter results are presented in Table 1. For the DISKPBB component, we find that the inner temperature and radial temperature index for this component are similar to those presented in Fürst et al. (2017): $T_{\rm in} = 2.8^{+0.5}_{-0.8}$ keV and $p = 0.57^{+0.04}_{-0.07}$. The latter is flatter than expected for a thin disk (which should give $p = 0.75$; Shakura & Sunyaev 1973), which could imply the presence of a thick, advection-dominated accretion disk, as expected for super-Eddington accretion (e.g., Abramowicz et al. 1988). There is a strong degeneracy between the stable DISKPBB component and the zero-point of the variations from the pulsed CUTOFFPL component, resulting in large errors on their respective normalizations/fluxes, as for the parameter combination found in the "pulse on"–"pulse-off" spectroscopy the DISKPBB model can produce a similar shape to the CUTOFFPL model. However, for the best-fit parameters, we find that the accretion column (the CUTOFFPL component) dominates the flux at the highest energies probed by *NuSTAR*, exactly where the high-energy power-law tail reported by Fürst et al. (2017) contributes in their model for the phase-averaged data.

Motivated by our results for NGC 7793 P13, which require two thermal blackbody components to fit the observed spectra (Walton et al. 2018), we also fit a second model in which the stable emission for NGC 5907 ULX consists of two thermal components: a thin disk (DISKBB) and a hotter blackbody (BB) component. As before, all the parameters for these components are the same for each phase bin. The global fit is also excellent with this model, χ^2/dof = 370/384, providing a reasonably good improvement over the DISKPBB case ($\Delta\chi^2 = 13$ for one additional free parameter). The parameter constraints for this model are also presented in Table 1, and we show the relative contribution of the model components for the peaks and the troughs of the pulse cycle in Figure 2. The strong

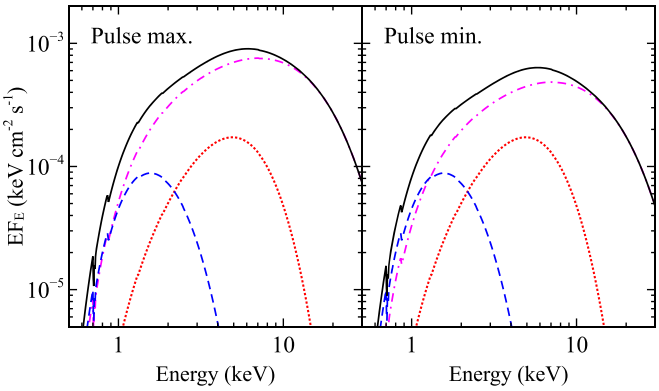

Figure 2. Relative contributions of the various spectral components during the peaks (left panel) and the troughs (right panel) of the pulse cycle from our phase-resolved analysis of NGC 5907 ULX with the DISKBB+BB +CUTOFFPL continuum model (similar to Figure 4 in Walton et al. 2018 for NGC 7793 P13). In both panels the total model is shown in solid black, the DISKBB and BB components (both steady) are shown in dashed blue and dotted red, respectively, and the CUTOFFPL component (pulsed) in dash-dot magenta. As the DISKBB and DISKPBB components are assumed to be steady across the pulse cycle, these components are identical in both panels.

degeneracy seen with the DISKPBB model is not present here, as neither the DISKBB or BB models can mimic the CUTOFFPL component, and the temperatures of the two thermal components ($kT \sim 0.4$ and $\sim$1.3 keV) are broadly similar to those seen with the same model in NGC 7793 P13 ($kT \sim 0.3$–0.5 and $\sim$1.1–1.5 keV). Here, we clearly see that the CUTOFFPL component associated with the accretion column dominates the highest observed energies.

3. The Broadband ULX Sample: Hard Excesses

Having established that the hard excesses in both NGC 7793 P13 and NGC 5907 ULX are associated with emission from the accretion columns (see also Walton et al. 2018), in this section we assess the presence of similar features in the rest of the ULX population. For this analysis, we focus on the sample with high-S/N broadband observations highlighted in Walton et al. (2018). These are sources for which *NuSTAR* has performed simultaneous observations with *XMM-Newton* and/or *Suzaku*

Table 2
Summary of the Hard Excess Detections in the ULX Population with Broadband Coverage to Date when the Lower-energy Data are Fit with Thermal Disk Models

Source	Distance (Mpc)	References	$N_{H,Gal}$ (K05) (10^{20} cm^{-2})	Hard Excess Detected?	References	Accretor
Circinus ULX5	4.2	F77	55.8	Yes	W13	Unknown
Holmberg II X-1	3.4	K02, T16	3.66	Yes	W15	Unknown
Holmberg IX X-1	3.6	P02, T16	5.54	Yes	W14, L16, W17b	Unknown
IC 342 X-1	3.4	S02, T16	29.9	Yes	This work	Unknown
IC 342 X-2	3.4	S02, T16	29.9	Yes	This work	Unknown
NGC 1313 X-1	4.2	M02, T16	4.13	Yes	This work	Unknown
NGC 5204 X-1	4.9	T16	1.75	Yes	M15	Unknown
NGC 5907 ULX1	17.1	T16	1.21	Yes	F17, this work	Neutron star
NGC 7793 P13	3.5	P10, T16	1.20	Yes	W17a	Neutron star

References. F77—Freeman et al. (1977), F17—Fürst et al. (2017), K02—Karachentsev et al. (2002), K05—Kalberla et al. (2005), L16—Luangtip et al. (2016), M02—Méndez et al. (2002), M15—Mukherjee et al. (2015), P02—Paturel et al. (2002), P10—Pietrzyński et al. (2010), S02—Saha et al. (2002), T16—Tully et al. (2016), W13-17b—Walton et al. (2013, 2014, 2015b, 2018, 2017).

(Mitsuda et al. 2007), resulting in a robust detection up to at least 20 keV, and which are not significantly confused with any other X-ray sources. In addition to the neutron star ULXs NGC 5907 ULX and NGC 7793 P13, the sample consists of Circinus ULX5 (Walton et al. 2013), Holmberg II X-1 (Walton et al. 2015b), Holmberg IX X-1 (Walton et al. 2014, 2017; Luangtip et al. 2016), IC 342 X-1 and X-2 (Rana et al. 2015), NGC 1313 X-1 (Bachetti et al. 2013; Miller et al. 2014; Walton et al. 2016), and NGC 5204 X-1 (Mukherjee et al. 2015). Details of all the observations considered in this work are given in Appendix A. We do not include M82 X-2 because, although we can isolate the pulsed emission, we cannot extract clean spectra of this source owing to its proximity to M82 X-1 (also absent from our sample). M82 X-1 is typically much brighter than X-2, reaching X-ray luminosities of up to $\sim 10^{41}$ erg s^{-1} (e.g., Kaaret et al. 2009; Brightman et al. 2016b).

Of the sources for which the nature of the accretor still remains unknown, hard excesses have already been reported in the literature for Circinus ULX5, Holmberg II X-1, Holmberg IX X-1, and NGC 5204 X-1 when the lower-energy data have been fit with thermal accretion disk models. Here, we assess whether similar features would also be required in the remaining sources, IC 342 X-1 and X-2 and NGC 1313 X-1, when fit with similar models. Since pulsations have not been detected for any of these sources, we fit their time-averaged spectra with an accretion disk model combining DISKBB +DISKPBB, allowing for an outer thin disk (exterior to R_{sp}; DISKBB) and an inner thick disk (DISKPBB; note that this is a slightly different model combination than the previous section, but has been frequently used in previous works). Neutral absorption is included as before (both Galactic and intrinsic; see Table 2 for the Galactic absorption columns). We then test whether these models require an additional high-energy continuum component by determining whether adding a phenomenological power-law tail to the hotter DISKPBB component (using the SIMPL model; Steiner et al. 2009) provides a significant improvement to the fit.

Figure 3 shows the residuals for the DISKBB+DISKPBB models for the three sources. Excesses are seen at the highest energies in all three cases, similar to those seen in the rest of the population, and we find that the addition of the SIMPL component provides a significant improvement to the fit with the DISKBB+DISKPBB continuum ($\Delta\chi^2 > 30$ for two additional dof). For NGC 1313 X-1, we stress that this is the case regardless of whether the atomic emission and absorption features associated with the ultrafast outflow reported in Pinto et al. (2016) and Walton et al. (2016) (which produce the residuals seen at $\sim$1 keV) are included in the model. We summarize the presence of these hard excesses in the broadband ULX population in Table 2. All the ULXs with broadband observations to date require an additional high-energy component when fit with dual-thermal disk models that may represent a super-Eddington accretion flow.

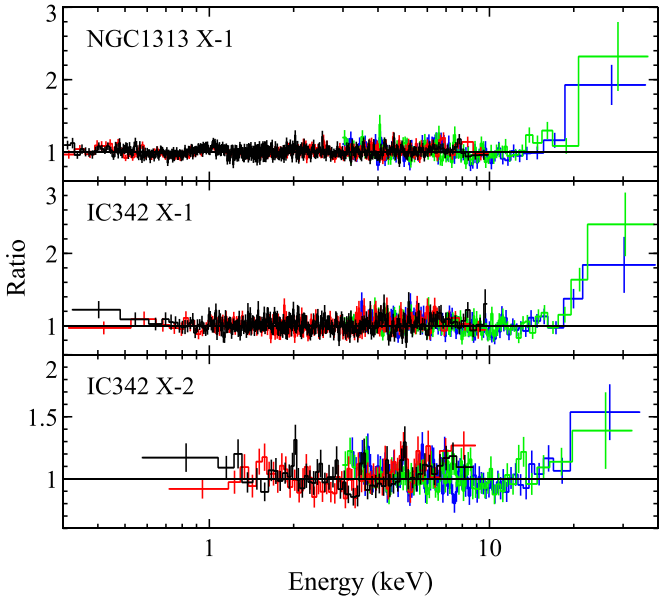

Figure 3. Data/model ratios to the DISKBB+DISKPBB continuum model for the ULXs NGC 1313 X-1 (top), IC 342 X-1 (middle), and IC 342 X-2 (bottom). The data from EPIC-pn, EPIC-MOS, FPMA, and FPMB are shown in black, red, green, and blue, respectively. In all three cases, excess emission is seen at the highest energies probed by *NuSTAR*. In the case of NGC 1313 X-1, the residuals at 1 keV are caused by the ultrafast outflow known in this source (Middleton et al. 2015; Pinto et al. 2016), and do not influence the presence of the hard excess.

4. The Broadband ULX Sample: ULX Pulsar Fits

We finish our analysis by testing whether the average spectra of the broadband ULX population can be well fit with a model similar to that applied to both NGC 7793 P13 and NGC 5907 ULX, continuing to focus on the broadband ULX sample

discussed in Section 3 for illustration. In particular, having demonstrated that even complex accretion disk models require an additional continuum component at the highest energies probed in all ULXs with broadband observations to date (Table 2), we wish to test whether these excesses can all be explained with emission from an accretion column similar to those seen in the three known ULX pulsars.

This is similar in concept to the recent works by Pintore et al. (2017) and Koliopanos et al. (2017). The former fit a model commonly applied to sub-Eddington pulsars to a sample of time-averaged *XMM-Newton* and *NuSTAR* ULX spectra, undertaking a broadband analysis where possible, and the latter fit a model motivated by the model for ULX pulsars proposed by Mushtukov et al. (2017, see below) to another sample of time-averaged ULX spectra, but do not undertake a full broadband analysis, instead treating the soft and hard X-ray data from *XMM-Newton* and *NuSTAR* separately. We stress that our analysis is strictly broadband (the soft and hard X-ray data are analyzed simultaneously), and the model used here is directly motivated by our observational analysis of the two ULX pulsars for which clean broadband spectroscopy is possible, and which have super-Eddington luminosities.

The model applied here consists of two thermal blackbody components for the accretion flow beyond $R_{\rm M}$, and a CUTOFFPL component for the accretion column, as required to fit the broadband data from NGC 7793 P13 (Walton et al. 2018) and also preferred by the data for NGC 5907 ULX (Section 2.2). As before, we allow for both Galactic and intrinsic neutral absorption. For the two known ULX pulsars in the sample, NGC 7793 P13 and NGC 5907 ULX, the shape parameters for the CUTOFFPL component are fixed to the best-fit values obtained for their pulsed emission ($\Gamma = 0.17$, $E_{\rm cut} = 4.7$ keV and $\Gamma = 0.7$, $E_{\rm cut} = 5.5$ keV, respectively; Figure 1). However, pulsations have not been detected for the majority of the sample, so we cannot isolate the emission from any accretion column present in these systems. In these cases, we set the shape parameters to the average values seen from the pulsed emission from the three ULX pulsars currently known: $\Gamma = 0.5$ and $E_{\rm cut} = 8.1$ keV (also shown in Figure 1).

For the thermal components, we construct a simple decision tree to determine which model components to fit in a systematic manner. Based on our analysis of NGC 7793 P13, we assume that $R_{\rm M} < R_{\rm sp}$, such that the thick inner disk can form before being truncated by the magnetic field. Initially, we therefore make use of the DISKBB+DISKPBB combination for the reasons discussed above (to remove any degeneracy between these components and prevent them from swapping temperatures, we set an upper limit for the DISKBB temperature of 1 keV in our fits). However, as discussed in Walton et al. (2018), if $R_{\rm sp}$ and $R_{\rm M}$ are similar, the thick inner disk may only extend over a small range of radii before being truncated by the magnetic field of the neutron star, and subsequently only emit over a relatively narrow range of temperatures. If this is the case then we should see a steeper radial temperature index (i.e., $p > 0.75$), as the DISKPBB model implicitly assumes that the emission from this component extends out to large radii (and therefore low temperatures), so increasing p is the only way the model can force the hotter component to be dominated by a small range of temperatures. In this case, the hotter component may be better described by a single blackbody (as appears to be the case for both NGC 7793 P13 and NGC 5907 ULX) than a disk component with a broad range of temperatures. Therefore, if we see that p runs up against its upper limit in fits with the DISKPBB component (we restrict the radial temperature index to the range $0.5 \leqslant p \leqslant 2.0$), we replace it with a BB component and present these fits instead.

Finally, to keep the models as simple as possible and minimize parameter degeneracies, we test to see whether both the thermal components are required by the data. Should the fit be similarly good after removing either of the thermal components included in the model, then we present these fits instead, retaining the component that provides the better fit of the two. However, where multiple epochs are considered for the same source (Holmberg IX X-1, NGC 5907 ULX) we also make sure to use the same model for all epochs for consistency, such that if one observation prefers two thermal components, while another does not, we still use the same two thermal components for all observations. For these sources, we also fit all of the observations considered simultaneously, allowing us to adopt a common neutral absorption column (e.g., Miller et al. 2013; Walton et al. 2017). We stress, however, that fully consistent results are obtained by allowing the column to vary between epochs.

The results are presented in Table 3, and we show the relative contributions of the model components for each of the spectra analyzed here in Figure 4. We also show the data/model ratios for the fits in Figure 5. For NGC 7793 P13, since the model applied here is identical to that used in our recent work focusing on this individual source, we take the results from Walton et al. (2018). Good broadband fits to the data are obtained in all cases, and critically we find that emission from a ULX pulsar-like accretion column can reproduce the hard X-ray *NuSTAR* data for all the sources for which the nature of the accretor currently remains unknown.

For most of the data sets considered, we fit the thermal continuum with the DISKBB+DISKPBB combination, and the radial temperature indices for the hotter DISKPBB component are flatter than expected for a thin disk. The exceptions are the two ULX pulsars (NGC 7793 P13, NGC 5907 ULX), Circinus ULX5, and IC 342 X-2. For both the ULX pulsars, we find that when using the DISKPBB model only a lower limit can be obtained on p, so we revert to a single blackbody for the hotter component. The only other source for which this is the case is IC 342 X-2, where we similarly switch from DISKPBB to a single BB. Here, we also find that the cooler DISKBB component is not required by the data, but we note that this is the most absorbed of the sources considered ($N_{\rm H;int} \sim 10^{22}$ cm^{-2}), so the fact that this component is not required could merely be related to the high levels of absorption. For Circinus ULX5, we also find that the DISKBB component is not required, but again this source is rather absorbed as the Galactic column toward Circinus is relatively high ($N_{\rm H;Gal} \sim 5.6 \times 10^{21}$ cm^{-2}, giving a total column of $\sim 8 \times 10^{21}$ cm^{-2}). However, in this case, we still find that the DISKPBB component prefers a fairly flat radial temperature index, similar to the bulk of the other data sets.

5. Discussion

The relative contributions of black hole and neutron star accretors to the ULX population are a matter of some debate. All three of the neutron star ULXs currently known have been discovered through the detection of coherent X-ray pulsations. Although simple searches have now been made for a broad

Table 3
Best-fit Parameters Obtained for the Fits to the Broadband ULX Sample with ULX Pulsar Models

Source	Thermal Continuum[a]	$N_{H;int}$ (10^{20} cm^{-2})	kT_1 (keV)	Norm$_1$	kT_2 (keV)	p	Norm$_2$[b]	CPL Flux[c]	χ^2/dof
N7793 P13	DBB+BB	$7.1^{+0.8}_{-0.7}$	0.48 ± 0.03	$0.80^{+0.19}_{-0.15}$	1.53 ± 0.04	⋯	$27.3^{+2.4}_{-2.2}$	$22.3^{+1.4}_{-1.6}$	1132/1159
Circ. ULX5	DPBB	21 ± 3	⋯	⋯	1.87 ± 0.07	0.71 ± 0.02	24^{+6}_{-4}	$6.7^{+1.2}_{-1.5}$	1216/1147
Ho II X-1	DBB+DPBB	$4.7^{+1.2}_{-1.0}$	$0.24^{+0.02}_{-0.01}$	32^{+11}_{-7}	$2.07^{+0.14}_{-0.12}$	0.56 ± 0.02	$3.6^{+1.5}_{-1.0}$	$4.7^{+0.6}_{-0.7}$	1954/1965
Ho IX X-1 (L)[d]	DBB+DPBB	16 ± 1	$0.31^{+0.03}_{-0.04}$	9^{+6}_{-3}	$2.7^{+0.5}_{-0.3}$	$0.63^{+0.08}_{-0.04}$	$2.4^{+3.2}_{-1.3}$	$20.3^{+2.9}_{-5.4}$	6268/5901
Ho IX X-1 (M)[d]	DBB+DPBB	⋯	0.27 ± 0.02	12^{+7}_{-4}	3.0 ± 0.2	0.54 ± 0.01	$1.4^{+0.4}_{-0.3}$	$20.0^{+2.0}_{-1.3}$	⋯
Ho IX X-1 (H)[d]	DBB+DPBB	⋯	$0.20^{+0.04}_{-0.03}$	36^{+51}_{-21}	1.92 ± 0.04	0.63 ± 0.01	34 ± 4	$20.2^{+1.0}_{-1.2}$	⋯
IC 342 X-1	DBB+DPBB	60^{+8}_{-5}	$0.36^{+0.04}_{-0.06}$	$3.6^{+4.8}_{-1.3}$	$2.1^{+0.3}_{-0.2}$	$0.63^{+0.08}_{-0.07}$	$3.2^{+2.8}_{-1.9}$	$8.3^{+0.5}_{-1.1}$	1351/1308
IC 342 X-2	BB	90^{+7}_{-6}	⋯	⋯	1.28 ± 0.05	⋯	9.8 ± 0.6	$10.8^{+0.5}_{-0.4}$	672/659
N1313 X-1	DBB+DPBB	22 ± 1	0.29 ± 0.01	$11.4^{+2.1}_{-0.9}$	$2.7^{+0.2}_{-0.3}$	$0.58^{+0.02}_{-0.01}$	$1.1^{+0.6}_{-0.4}$	$4.6^{+0.8}_{-1.2}$	1840/1691
N5204 X-1	DBB+DPBB	$2.8^{+1.5}_{-1.4}$	$0.27^{+0.02}_{-0.03}$	$7.1^{+3.4}_{-2.1}$	1.8 ± 0.2	$0.64^{+0.11}_{-0.06}$	$2.8^{+3.7}_{-1.4}$	$1.8^{+0.4}_{-0.5}$	548/520
N5907 ULX1 (L)[d]	DBB+BB	66^{+8}_{-2}	$0.46^{+0.07}_{-0.09}$	$0.39^{+0.70}_{-0.17}$	$1.19^{+0.14}_{-0.19}$	⋯	3.2 ± 0.8	$2.6^{+0.7}_{-0.8}$	598/646
N5907 ULX1 (H)[d]	DBB+BB	⋯	$0.50^{+0.09}_{-0.11}$	$0.30^{+0.76}_{-0.15}$	$1.31^{+0.14}_{-0.19}$	⋯	$4.2^{+1.5}_{-1.4}$	13.5 ± 1.2	⋯

Notes.
[a] DBB—DISKBB, DPBB—DISKPBB, BB—blackbody. Where two thermal components are used, the DISKBB is always the cooler of the two (kT_1, Norm$_1$), with its temperature limited to be <1 keV to reduce degeneracy between the components.
[b] For the DISKPBB model the normalization is given in units of 10^{-3}, and for the BB model it is given in units of 10^{-6}.
[c] CPL—CUTOFFPL. The shape parameters for this component are fixed (see Section 4), and the 2–10 keV fluxes are given in units of 10^{-13} erg cm^{-2} s^{-1}.
[d] For sources where multiple observations are considered, we assume a common $N_{H;int}$ across all epochs; the χ^2 quoted is for the combined fit.

section of the ULX population (e.g., Doroshenko et al. 2015, Appendix B), pulsations have not been seen from any other ULX to date. However, these signals can be difficult to find. Being extragalactic, ULXs are typically faint, resulting in low count rates. In addition, motions of the neutron star within its binary orbit (the parameters of which are not generally known a priori) can shift the frequency the pulsations should be observed at across the duration of individual observations. Both of these issues can hinder the detection of pulsations, even if they are intrinsically present. Furthermore, in 2/3 of the ULX pulsars known, where we know the pulsations are detectable and constraints on the binary orbit have subsequently been obtained, the pulsations are transient. In M82 X-2, for example, the duty cycle of the pulsations is <50%. Additional means of identifying neutron star ULXs beyond the detection of pulsations may therefore be key to addressing their contribution to the overall ULX population.

Walton et al. (2018) discuss the qualitative similarity of the broadband spectra of all the ULXs observed with clean, high-S/N broadband spectra, i.e., combining *NuSTAR* with either *XMM-Newton* and/or *Suzaku*. This sample consists of known ULX pulsars (NGC 7793 P13 and NGC 5907 ULX), as well as ULX with unknown accretors (Circinus ULX5, Holmberg II X-1, Holmberg IX X-1, IC 342 X-1 and X-2, NGC 1313 X-1, and NGC 5204 X-1; see Section 3). Here, we have demonstrated that *all* these sources require an additional high-energy continuum component that dominates above ∼10 keV when the lower-energy data are modeled with thermal accretion disk models. We note that, based on their analysis of *NuSTAR* data for a number of the sources considered here, Koliopanos et al. (2017) suggest that the need for this additional component is an artefact of mis-modeling the hotter (∼2–3 keV) thermal emission. Fitting the 4–30 keV data with a simple DISKBB model, they find that an additional high-energy component would be required, but after switching to the more complex DISKPBB model they find that this is no longer the case. However, this is clearly a consequence of the limited bandpass considered by these authors; the DISKPBB model has routinely been used to fit this thermal emission, both in this work and in the existing literature (e.g., Mukherjee et al. 2015; Walton et al. 2015b, 2017), and when fitting the full ∼0.3–30 keV broadband data an additional high-energy component is still required.

In both NGC 7793 P13 and NGC 5907 ULX1, based on phase-resolved analyses, we find that the additional high-energy emission is pulsed and therefore associated with the magnetically collimated accretion columns that must be present in these sources. Although we cannot separate the broadband X-ray emission from M82 X-1 and X-2, and as such these sources are not in our sample, we do note that the pulsed emission from M82 X-2 also has a very similar spectral form as NGC 7793 P13 and NGC 5907 ULX (Brightman et al. 2016a), with significant emission in high-energy X-rays (and we note that there is some evidence for a hard excess in M82 X-1 as well; Brightman et al. 2016b).

If the presence of a hard excess is an indication that the central accretion operates in this manner, then the fact that the entire sample shows this feature is consistent with them all hosting neutron star accretors. Indeed, fitting the broadband data with a model inspired by that required to fit the known ULX pulsars, in which the highest-energy emission probed by *NuSTAR* is dominated by an accretion column similar to those seen in the ULX pulsar systems, provides a good fit to the available high-energy data in all cases.

5.1. Accretion Geometry and the Lack of Pulsations

Our fits suggest why, even if they are all neutron stars, pulsations have not been seen in any cases other than NGC 7793 P13 and NGC 5907 ULX among the sample considered here (e.g., Doroshenko et al. 2015, Appendix B). The final model applied to the broadband data here (typically) consists of two thermal components, which we assume arise in the accretion flow beyond R_M (with the cooler component arising in the regions of the disk beyond R_{sp}, and the hotter component the regions between R_{sp} and R_M), and a high-energy continuum (modeled with a CUTOFFPL component)

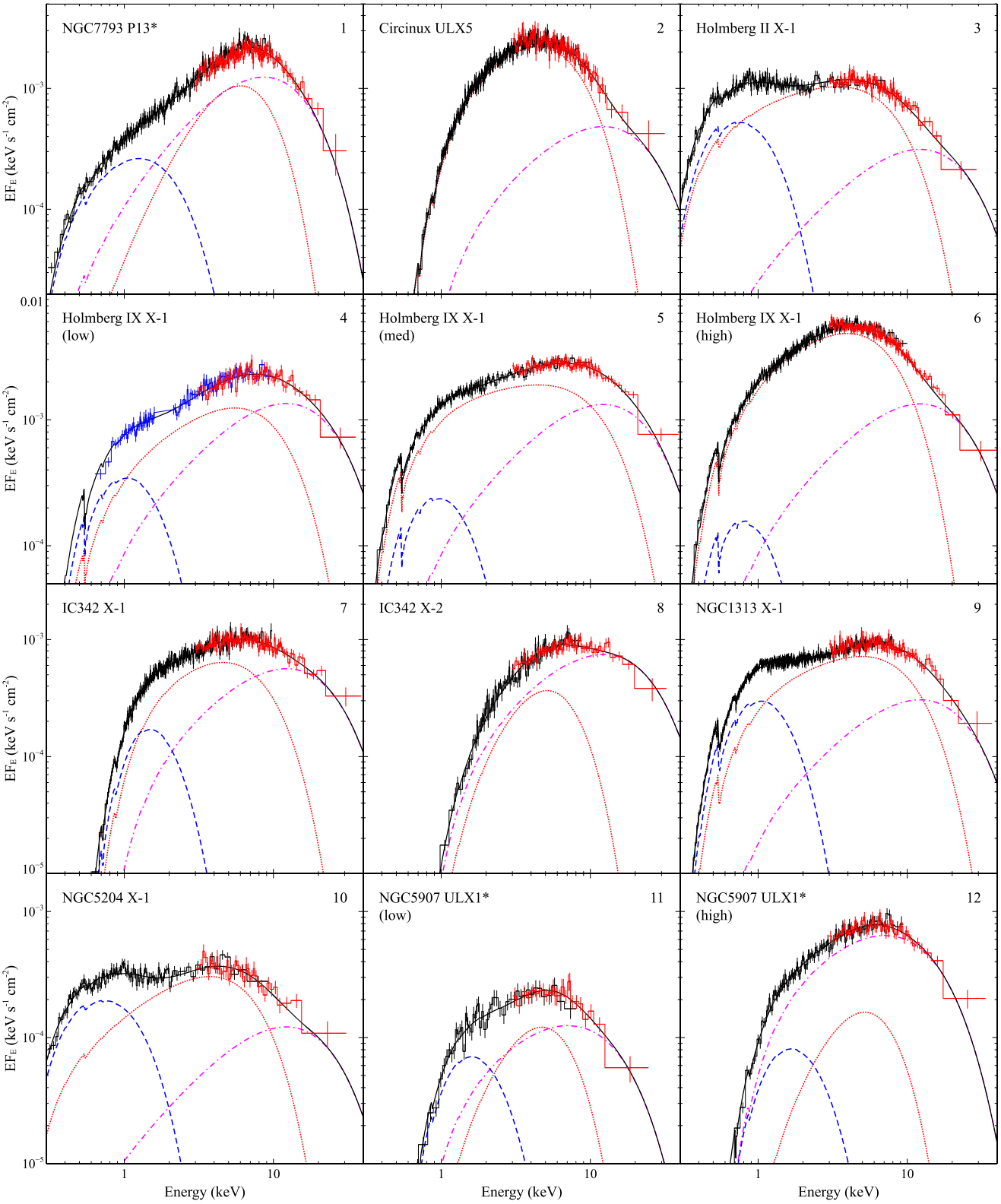

Figure 4. Broadband spectra of the ULX population with simultaneous coverage in soft (*XMM-Newton*, *Suzaku*) and hard (*NuSTAR*) X-rays, and the relative contributions of the various model components included in our fits based on the known ULX pulsars (indicated with an asterisk). We show the same observations as Figure 11 from Walton et al. (2018, as before, *XMM-Newton* EPIC-pn data are in black, *Suzaku* front-illuminated XIS data are in blue, and *NuSTAR* data are in red), and keep the same ordering of the panels for ease of comparison, but here the data have been unfolded through the best-fit model for each source (solid black line). These models generally include two thermal components likely from the accretion flow beyond R_M, with the cooler shown in dashed blue (modeled with DISKBB; note that on occasion this component is not required) and the hotter shown in dotted red (modeled with either DISKPBB or a single blackbody), and a high-energy component representing emission from a ULX pulsar-like accretion column, which is shown in dash-dot magenta (modeled with a CUTOFFPL component); see Section 4 for individual source details. Where multiple observations of the same source are shown, the relative fluxes of these data sets are indicated in parentheses.

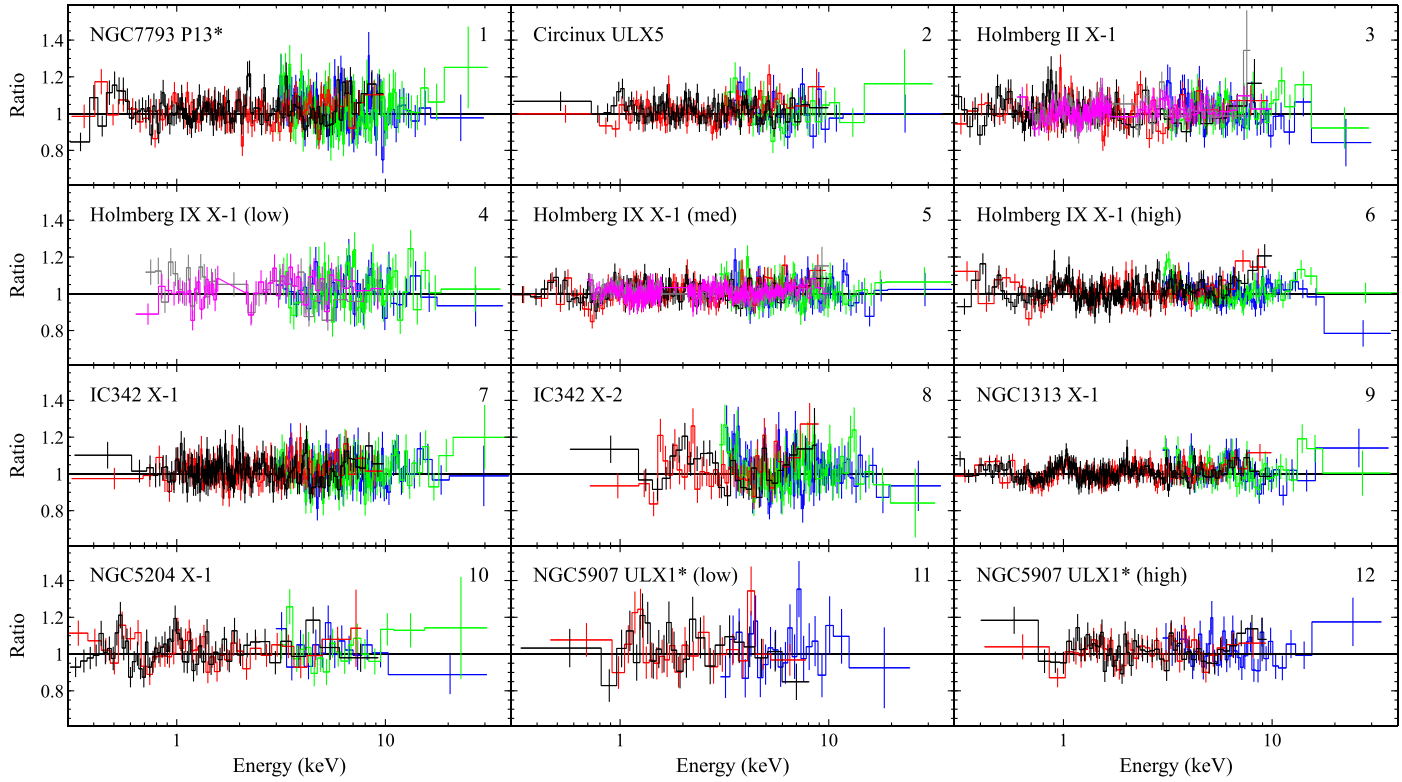

Figure 5. Data/model ratios for our ULX pulsar fits to the broadband ULX sample (see Section 4); the panel ordering and source/observation nomenclature are the same as Figure 4. Here, we show the full data set fit in each case, with data from EPIC-pn and EPIC-MOS (both *XMM-Newton*), the front- and back-illuminated XIS (both *Suzaku*), and FPMA and FPMB (both *NuSTAR*) shown in black, red, magenta, gray, green, and blue, respectively (in the case of NGC 5907 ULX, the combined FPMA+FPMB data are shown in blue). The data have been further rebinned for visual purposes.

from the accretion column. Although the accretion column is always required in our fits to account for the hard excesses in the data, from Figure 4 it is clear that among the rest of the sample this generally makes a smaller relative contribution to the total emission than for the two observations of the known ULX pulsars from which pulsations have been detected, sometimes substantially so. To quantitatively illustrate this, we summarize the total 0.3–40.0 keV observed fluxes ($F_{\rm tot}$) and the fluxes inferred for the CUTOFFPL component alone ($F_{\rm col}$) in Table 4, and highlight the observations where pulsations have been detected. We stress that these fits are only supposed to be illustrative, since we do not actually know the precise spectral form of any accretion columns present in the remaining sample, and substantial deviations from our assumed shape could lead to larger errors than the simple statistical errors computed given this shape (see below). Nevertheless, the fluxes confirm the visual conclusion from Figure 4; for the observations in which pulsations have been detected our analysis suggests that that the column has provided $\sim$60% or more of the total observed flux, while for sources in which pulsations have not currently been detected we generally infer much lower values than this. The pulse fractions for the majority of the rest of the sample would therefore be diluted in comparison to both NGC 7793 P13 and NGC 5907 ULX, and therefore any pulsations would be harder to detect even before any S/N considerations.

The only exception is IC 342 X-2, where we would infer a relative contribution from the column to the total flux similar to the known pulsar ULXs. Is it also interesting to note that this is the only other source for which we find the DISKPBB component prefers a radial temperature index steeper than a standard thin disk, so that it can be replaced with a single blackbody (see Section 4). In Walton et al. (2018) we suggested that this could be an indication that the magnetic field of the neutron star truncates the disk fairly close to the point that it becomes locally Eddington (i.e., $R_{\rm M} \sim R_{\rm sp}$), such that the thick inner disk only extends over a small range of radii and subsequently emits over a narrow range of temperatures.

Table 4
Comparison of the the Total Observed Flux and the Flux from the Observed/Potential Accretion Columns in the 0.3–40 keV Band Based on the ULX Pulsar Fits for the Data Sets Considered in this Work

Data Set	$F_{\rm tot}$ (10^{-12} erg cm^{-2} s^{-1})	$F_{\rm col}$	$F_{\rm col}/F_{\rm tot}$
Circ ULX5	73.5 ± 1.3	$14.8^{+2.6}_{-3.6}$	$0.20^{+0.03}_{-0.04}$
Ho II X-1	60.4 ± 0.9	$10.4^{+1.4}_{-1.6}$	$0.17^{+0.02}_{-0.03}$
Ho IX X-1 (L)	$91.6^{+2.2}_{-2.3}$	$44.3^{+6.4}_{-11.7}$	0.48^{+7}_{-13}
Ho IX X-1 (M)	123.0 ± 1.4	$43.4^{+4.3}_{-5.8}$	$0.35^{+0.04}_{-0.05}$
Ho IX X-1 (H)	199.5 ± 1.8	$43.9^{+2.4}_{-2.5}$	0.22 ± 0.01
IC 342 X-1	37.9 ± 0.6	$17.8^{+1.1}_{-2.2}$	$0.47^{+0.03}_{-0.06}$
IC 342 X-2	30.7 ± 0.8	23.4 ± 1.0	0.76 ± 0.04
N1313 X-1	40.2 ± 0.5	$10.0^{+1.8}_{-2.6}$	$0.25^{+0.04}_{-0.07}$
N5204 X-1	18.5 ± 0.5	$4.1^{+0.7}_{-1.2}$	$0.22^{+0.04}_{-0.06}$
N5907 ULX1 (L)	7.7 ± 0.4	$4.1^{+0.9}_{-1.3}$	$0.53^{+0.13}_{-0.17}$
N5907 ULX1 (H)[a]	$25.7^{+0.7}_{-0.6}$	$21.2^{+1.7}_{-2.0}$	$0.82^{+0.07}_{-0.08}$
N7793 P13[a]	67.0 ± 1.1	$39.7^{+2.6}_{-2.9}$	0.59 ± 0.04

Note.
[a] Data sets for which pulsations have been detected (note that pulsations were only detected in the higher-flux observation of NGC 5907 ULX1).

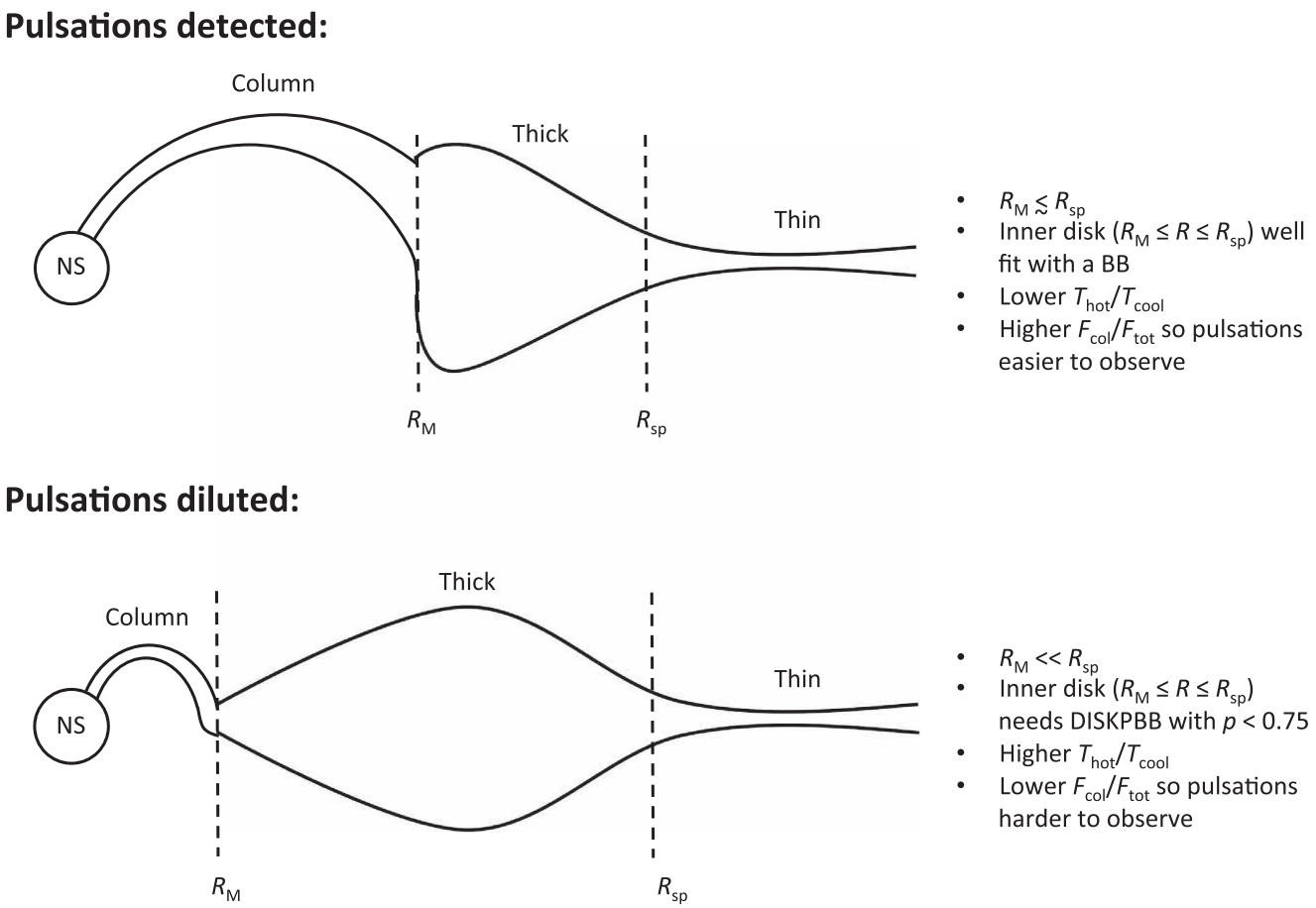

Figure 6. Schematic diagram illustrating the potential difference between the pulsar ULXs (top) and the ULXs for which pulsations have not been detected (bottom), assuming neutron star accretors (not to scale). In the former case, the magnetic field of the neutron star truncates the disk relatively close to the spherization radius, resulting in the thick inner disk spanning a narrow range of radii and a stronger relative contribution from the emission from the accretion column, making pulsations easier to detect. In the latter case, the disk is truncated at radii much smaller than the spherization radius, allowing the thick inner disk to span a broad range of radii and resulting in a weaker relative contribution from the accretion column, in turn making pulsations harder to detect. In this case, the structure of the disk should be very similar to that calculated for the black hole case (e.g., Poutanen et al. 2007; Dotan & Shaviv 2011).

This was also supported by the rough similarity (within a factor of ∼5) of the characteristic radii estimated for both the DISKBB and BB components for NGC 7793 P13 and we speculated that this might therefore be an indicator of a neutron star accretor since such truncation would not be possible for black hole systems. King et al. (2017) suggest that $R_M \sim R_{sp}$ may be a necessary requirement for the detection of pulsations, since the steady (i.e., non-pulsed) emission from the accretion flow beyond R_M dilutes the pulsations less, consistent with our NGC 7793 P13 results. We note again that IC 342 X-2 is the most absorbed of the sources considered, with a rather substantial column density ($\sim 10^{22}$ cm^{-2}), and we have been forced to assume a spectral form for the accretion column. In combination, these could potentially lead to large uncertainties in our continuum fits (see below). Nevertheless, although nothing has been detected to date, IC 342 X-2 might therefore be an interesting source for future pulsation searches.

However, we stress that for the other sources, where we obtain flatter radial temperature indices ($p < 0.75$), this would not exclude neutron star accretors. We expect that this would suggest that $R_M \ll R_{sp}$ in these cases, such that the thick inner disk extends over a sufficiently large range of radii/temperatures that the model returns values in line with the broad expectations for such an accretion flow. This would potentially explain why the accretion column appears to be weaker in a relative sense in these cases, as the flow beyond R_M dominates more of the observed emission, and is qualitatively consistent with the above suggestion from King et al. (2017) given the lack of pulsations detected from these systems. In order for $R_M \ll R_{sp}$, either the accretion rate ($\dot{M}$) must be substantially higher, or the magnetic field substantially weaker in these systems in comparison to those where $R_M \sim R_{sp}$, as $R_M \propto \dot{M}^{-2/7} B^{4/7}$ (Lamb et al. 1973; Cui 1997)[10] and $R_{sp} \propto \dot{M}$ (Shakura & Sunyaev 1973). A rough schematic diagram of the potential difference between the known pulsar ULXs and sources for which pulsations have not been detected is shown in Figure 6.

Mushtukov et al. (2017) and Koliopanos et al. (2017) discuss an alternative scenario. In their picture, the hotter thermal component arises in the accretion "curtain" formed just interior to R_M as the accreting material begins to follow the field lines; the cooler of the thermal components represents the innermost regions of the disk, just outside of R_M. Based on their calculations, Mushtukov et al. (2017) argue that this curtain should be optically thick, and would have the appearance of a

[10] We note the caveat that these models assume the disk outside R_M is thin, which may not be the case in these systems. However, we expect that the qualitative dependencies between R_M and $\dot{M}$ and B (i.e., higher B resulting in a larger R_M) are likely robust to this issue.

multi-color blackbody (similar to an accretion disk), consistent with the two thermal components typically seen in ULX spectra. In this case, the radius of the cooler component corresponds to $R_{\rm M}$. However, we note the strong similarity of the radius of the cooler thermal component in NGC 7793 P13 and the co-rotation radius (the point in the disk at which the accreting material co-rotates with the neutron star; $R_{\rm co}$) in this source (Walton et al. 2018), which is likely problematic for this scenario. Since accretion must be occurring in these systems we know that $R_{\rm M} < R_{\rm co}$, otherwise the source would be in the "propeller" regime in which the magnetic field prohibits accretion.

We further test the scenario proposed here by comparing the relative temperatures and radii of the two thermal components across the full sample considered here. Unfortunately, since the DISKBB component is not required in the fits for IC 342 X-2 and Circinus ULX5 (potentially related to the high levels of absorption in these cases) we cannot provide a reasonable comparison for these sources, but for the rest of the sample we compute the characteristic radii of the hotter (DISKPBB/BB, as appropriate) and cooler (DISKBB) components, similar to Walton et al. (2018). For the BB radii, we use standard blackbody theory, while for both the DISKBB and DISKPBB models the normalization is proportional to $R_{\rm in}^2 \cos\theta / f_{\rm col}^4$ (where $R_{\rm in}$ and θ are the inner radius and the inclination of the disk, and $f_{\rm col}$ is the color correction factor relating the observed "color" temperature to the effective blackbody temperature of the disk: $T_{\rm col} = f_{\rm col} T_{\rm eff}$). In order to mimic our estimates for NGC 7793 P13, we assume that $\cos\theta = f_{\rm col} = 1$ (i.e., a face-on disk with no color correction). As long as $f_{\rm col}$ and θ are similar for both the inner and outer regions of the disk, the exact values of these quantities should not strongly influence our estimates of the *relative* radii of the two components.

In all cases, we find that the radii of the hotter components are smaller than the cooler ones, as expected. For NGC 5907 ULX, the radii differ by a factor of $R_{\rm cool}/R_{\rm hot} \sim 6$, similar to NGC 7793 P13. However, for the remaining sample, all of which required a DISKPBB component with $p < 0.75$ for the hotter component, the differences are much larger, and are typically $R_{\rm cool}/R_{\rm hot} \sim 50$. We stress that these comparisons are only very rough, as issues such as beaming have not been accounted for (thus we do not compute formal errors). However, if the thick inner disk does extend over a broader range of radii (i.e., closer to the neutron star) in the ULXs for which pulsations have not been detected, then for these sources we would also expect the temperature of the hotter thermal component to be higher than that of the cooler component. Indeed, for the known ULX pulsars we find that the ratio $T_{\rm hot}/T_{\rm cool} \sim 3$, while for the rest of the general ULX population (where this can be tested) we find this ratio is $\sim$7.

To test whether these results are robust to the potential systematic issues introduced by assuming a spectral shape for the accretion column, we investigate how the results change for the known pulsar ULXs when the CUTOFFPL component from the accretion column is assumed to have the average values for Γ and $E_{\rm cut}$ used for the rest of the sample, rather than their individually constrained spectral shapes. In addition, using Holmberg II X-1 as a randomly selected test case, we also investigate how the results change when we force the CUTOFFPL component to have same Γ and $E_{\rm cut}$ as M82 X-2, NGC 7793 P13 and NGC 5907 ULX in turn (instead of their averages). With these tests we find that, on average, $F_{\rm col}/F_{\rm tot}$ changes by $\sim$80%, $R_{\rm cool}/R_{\rm hot}$ changes by $\sim$25% and $T_{\rm hot}/T_{\rm cool}$ changes by $\sim$10% (where errors are given in the form $\Delta x/x$) relative to the results presented above.

Clearly the assumption made about the spectral shape of the accretion column can have a significant effect on the relative contribution inferred for this emission. However, we would have to be systematically underestimating $F_{\rm col}/F_{\rm tot}$ for the unknown ULXs in order for these sources to be similar to the known ULX pulsars in this regard. However, for the tests performed with Holmberg II X-1 (discussed above), we find that when adopting the different parameter combinations from M82 X-2, NGC 7793 P13, and NGC 5907 ULX for the accretion column $F_{\rm col}/F_{\rm tot}$ both increases and decreases (depending on the parameter combination used) in comparison to the results obtained assuming their average spectral form. Adopting this average spectral form for the rest of the ULX sample is therefore unlikely to systematically bias $F_{\rm col}/F_{\rm tot}$ toward lower values. Furthermore, the average changes in $R_{\rm cool}/R_{\rm hot}$ and $T_{\rm hot}/T_{\rm cool}$ are too small to change the general conclusions discussed above.

The results presented here are therefore consistent with the idea that the main difference between the sources where steeper and flatter radial temperature indices are preferred for the hotter component is simply that $R_{\rm sp}$ and $R_{\rm M}$ are closer together in the former case, as suggested in Figure 6, making pulsations easier to detect. Since the former implies significant truncation by the magnetic field, this further supports the idea that steep radial temperature indices could also potentially indicate ULX pulsar candidates.

5.2. ULX Demographics

Other works have recently attempted to address the demographics of the ULX population through theoretical considerations. Middleton & King (2017) consider the impact of geometrical beaming on the demographics of flux-limited ULX samples within the framework of a model in which the beaming increases with (Eddington-scaled) accretion rate. The results are strongly dependent on the relative spatial number densities of neutron stars and black holes, which are not currently known. However, if this is skewed in favor of neutron stars, then scenarios in which flux-limited samples are dominated by such sources are certainly possible. Although the sample considered here is not formally well defined in a statistical sense, it would most likely be similar to the flux-limited case. Wiktorowicz et al. (2017) also consider this question from a stellar evolution standpoint, performing a suite of binary population synthesis simulations. Here, the results depend quite strongly on the star formation history and also somewhat on the metallicity of the host galaxies in which the ULXs reside. Continued star formation will likely produce a ULX population dominated by neutron stars, while brief bursts of star formation will likely produce a ULX population dominated by black holes. In addition, lowering the metallicity increases the preference for black hole systems. These calculations suggest that there are scenarios in which the sample considered here could be dominated by neutron stars. Both of these theoretical approaches are therefore consistent with the observational analysis presented here.

The calculations by Wiktorowicz et al. (2017) may also offer other potential means to identify neutron star accretors among the ULX population. Their simulations suggest there is a

channel through which the onset of a ULX phase can occur late in the evolution of the binary system for neutron star accretors that is not available for black holes. They predict that ULXs with evolved counterparts (red giants/supergiants; RGs/RSGs) should only be produced by neutron star systems. A number of ULXs with confirmed RSG counterparts have now been discovered (Heida et al. 2015, 2016), with a number of additional candidates also identified (Heida et al. 2014; López et al. 2017). Neutron star accretors would provide a natural explanation for the lack of significant variations in the radial velocities (RVs) of the counterparts where multiple epochs of high-S/N spectroscopy are available (Heida et al. 2016) as the RSG would dominate the total mass of the system, further supporting this prediction.

5.3. Black Hole ULXs

Although the *NuSTAR* ULX sample is consistent with being dominated by neutron star accretors, it is still possible that black hole ULXs do exist. However, to date there is only one[11] ULX, M101 ULX-1, in which the binary mass function is claimed to require a black hole accretor ($M > 5\ M_{\odot}$; Liu et al. 2013), but this is based on a very poorly sampled RV curve. Perhaps more critically, the RV data have been compiled from He II emission assumed to arise from its Wolf-Rayet binary companion, which may lead to unreliable mass estimates (e.g., Laycock et al. 2015). Unfortunately, this source is not accessible to *NuSTAR*, as its spectrum is extremely soft; the source is frequently undetected above ∼5 keV (e.g., Soria & Kong 2016). Within the framework of high/super-Eddington accretion in which a thick, inner funnel forms in the accretion flow, this is interpreted as the source being viewed close to edge-on, such that the large scale-height regions of the flow obscure the hottest inner regions that would otherwise dominate the *NuSTAR* band from direct view (e.g., Sutton et al. 2013b; Middleton et al. 2015; Pinto et al. 2017).

It is interesting to note that, although all the observed spectra are qualitatively similar at the highest energies, where the accretion column dominates in the known pulsars, there are still differences in this band between sources in the *NuSTAR* sample in terms of their long-term variability between observing epochs (typically probing ∼month–year timescales). In Walton et al. (2017) we found that in the case of Holmberg IX X-1 the highest energies ($\gtrsim$15 keV) remained remarkably constant between observing epochs, despite strong variability at lower energies. In contrast, Fürst et al. (2017) found that the high-energy emission in NGC 5907 ULX varied strongly in correlation with its lower-energy emission. Whether this difference could be related to different central accretors (black hole versus neutron star), or whether it could merely be a result of, e.g., different viewing angles remains to be seen. Robust identification of black hole ULXs that are accessible to *NuSTAR* will be necessary to investigate this further.

[11] The hyperluminous X-ray source ESO 243–49 HLX1 is also widely expected to be a black hole (being the best known candidate for an intermediate-mass black hole, with $M \sim 10^4\ M_{\odot}$). However, this is a clear outlier among the broader ULX population owing to its truly extreme luminosity ($L_{\rm X,peak} \sim 10^{42}$ erg s^{-1}; Farrell et al. 2009), the fact that it exhibits X-ray spectral and state-transitions consistent with known sub-Eddington behavior (Davis et al. 2011; Servillat et al. 2011; Webb et al. 2012), and its (quasi-) periodic outbursts (Godet et al. 2014; Soria et al. 2017). Instead, it is considered likely that this is the stripped nucleus of a dwarf galaxy falling into ESO 243–49. However, all of the methods for estimating the mass currently available here rely on indirect scaling relations.

6. Summary and Conclusions

We have undertaken a phase-resolved analysis of the ULX pulsar NGC 5907 ULX, following on from our work on the other two known ULX pulsars, M82 X-2 and NGC 7793 P13. We find that the spectral form of the pulsed emission from the accretion column is broadly similar in all three sources (a very hard rise, before turning over to a steep spectrum at high energies). Furthermore, we find that this emission component dominates the total emission at the highest energies probed, resulting in the hard excesses observed in these sources when the lower-energy data are fit with accretion disk models. Extending our consideration to the full sample of ULXs with broadband coverage to date, we find that similar hard excesses are observed in *all* the sources in this sample. For the ULXs where the nature of the accretor is currently unknown (the majority of the sources considered here), we investigate whether these hard excesses are all consistent with being produced by an accretion column similar to those present in the known ULX pulsars. We find that in all cases a similar accretion column can successfully reproduce the observed data, using the average shape of the pulsed emission in M82 X-2, NGC 7793 P13, and NGC 5907 ULX as a template. This is consistent with the hypothesis that the broadband ULX sample is dominated by neutron star accretors. For the unknown ULXs, our spectral fits suggest that the relative contribution of the non-pulsed emission from the accretion flow beyond the magnetosphere in comparison to that associated with the accretion columns is larger than observed in the known pulsar ULXs. This may help to explain the lack of pulsations detected from these sources, assuming that they are also powered by neutron star accretors.

The authors would like to thank the reviewer for positive feedback which helped to improve the final manuscript. D.J.W. and M.J.M. acknowledge support from STFC Ernest Rutherford fellowships, A.C.F. acknowledges support from ERC Advanced Grant 340442, and D.B. acknowledges financial support from the French Space Agency (CNES). This research has made use of data obtained with *NuSTAR*, a project led by Caltech, funded by NASA and managed by NASA/JPL, and has utilized the NUSTARDAS software package, jointly developed by the ASDC (Italy) and Caltech (USA). This work has also made use of data obtained with *XMM-Newton*, an ESA science mission with instruments and contributions directly funded by ESA Member States, and with *Suzaku*, a collaborative mission between the space agencies of Japan (JAXA) and the USA (NASA).

Facilities: NuSTAR, *XMM*, *Suzaku*.

Appendix A
Broadband Observation Log

Table 5 gives the key details for the *XMM-Newton*, *NuSTAR* and *Suzaku* observations that comprise the broadband ULX data sets considered in this work.

Appendix B
NuSTAR Pulsation Search

The *XMM-Newton* data considered in this work have been systematically searched for pulsations by either Doroshenko et al. (2015) and/or the ExTRAS variability survey[12] (De Luca et al. 2016). Aside from the known pulsar systems, no further

[12] http://www.extras-fp7.eu/index.php

Table 5
Details of the Broadband ULX Observations

Data Set	Date (approx.)	OBSID(s)			Integrated Good Exposures (ks)		
		XMM-Newton	*Suzaku*	*NuSTAR*	*XMM-Newton*[a]	*Suzaku*	*NuSTAR*
Circinus ULX5	2013 Feb	0701981001	⋯	30002038004	37/47	⋯	47
Holmberg II X-1	2013 Sep	0724810101/301	708015010/20	30001031002/3/5	10/23	90	262
Holmberg IX X-1 (low)	2015 Apr	⋯	707019030	30002034006	⋯	35	64
Holmberg IX X-1 (med)	2012 Oct	0693850801/0901/1001	707019020/30/40	30002033002/3	17/35	324	167
Holmberg IX X-1 (high)	2012 Nov	0693851101/1701/1801	⋯	30002033005/06/08/10	17/24	⋯	167
IC 342 X-1	2012 Aug	0693850601/1301	⋯	30002032003/5	70/84	⋯	329
IC 342 X-2	2012 Aug	0693850601/1301	⋯	30002032003/5	70/84	⋯	329
NGC 1313 X-1	2012 Dec	0693850501/1201	⋯	30002035002/4	164/231	⋯	360
NGC 5204 X-1	2013 Apr	0693850701/1401	⋯	30002037002/4	24/30	⋯	211
NGC 5907 ULX1 (low)	2013 Nov	0724810401	⋯	30002039005	20/32	⋯	123
NGC 5907 ULX1 (high)	2014 Jul	0729561301	⋯	80001042002/4	38/43	⋯	132
NGC 7793 P13	2016 May	0781800101	⋯	80201010002	28/46	⋯	114

Note.
[a] *XMM-Newton* exposures are listed for the EPIC-pn/MOS detectors.

coherent signals have been significantly detected in the rest of the broadband ULX sample to date. We have also extended these searches into the *NuSTAR* data considered here, following the approach taken in Fürst et al. (2016) for NGC 7793 P13. For each *NuSTAR* data set we calculated power spectral densities based on 3–40 keV light curves with 0.05 s resolution; all times were transferred to the solar barycenter using the DE200 solar ephemeris. We searched the complete available frequency range up to a maximum frequency of 10 Hz using the ACCELSEARCH routine in PRESTO (Ransom et al. 2002), following the approach pioneered in Bachetti et al. (2014). Aside from the known pulsar systems, no significant excess over the Poisson noise was found in any observation for any other source considered here, even when allowing for a period derivative in these searches. This is consistent with the results from *XMM-Newton*.

ORCID iDs

D. J. Walton https://orcid.org/0000-0001-5819-3552
F. Fürst https://orcid.org/0000-0003-0388-0560
M. Heida https://orcid.org/0000-0002-1082-7496
F. A. Harrison https://orcid.org/0000-0003-2992-8024
D. Barret https://orcid.org/0000-0002-0393-9190
D. Stern https://orcid.org/0000-0003-2686-9241
M. Bachetti https://orcid.org/0000-0002-4576-9337
M. Brightman https://orcid.org/0000-0002-8147-2602
A. C. Fabian https://orcid.org/0000-0002-9378-4072
M. J. Middleton https://orcid.org/0000-0002-8183-2970

References

Abramowicz, M. A., Czerny, B., Lasota, J. P., & Szuszkiewicz, E. 1988, ApJ, 332, 646
Bachetti, M., Harrison, F. A., Walton, D. J., et al. 2014, Nat, 514, 202
Bachetti, M., Rana, V., Walton, D. J., et al. 2013, ApJ, 778, 163
Brightman, M., Harrison, F., Walton, D. J., et al. 2016a, ApJ, 816, 60
Brightman, M., Harrison, F. A., Barret, D., et al. 2016b, ApJ, 829, 28
Cui, W. 1997, ApJ, 482, L163
Davis, S. W., Narayan, R., Zhu, Y., et al. 2011, ApJ, 734, 111
De Luca, A., Salvaterra, R., Tiengo, A., et al. 2016, ApSSP, 42, 291
Doroshenko, V., Santangelo, A., & Ducci, L. 2015, A&A, 579, A22
Dotan, C., & Shaviv, N. J. 2011, MNRAS, 413, 1623
Farrell, S. A., Webb, N. A., Barret, D., Godet, O., & Rodrigues, J. M. 2009, Nat, 460, 73
Freeman, K. C., Karlsson, B., Lynga, G., et al. 1977, A&A, 55, 445
Fürst, F., Walton, D. J., Harrison, F. A., et al. 2016, ApJ, 831, L14
Fürst, F., Walton, D. J., Stern, D., et al. 2017, ApJ, 834, 77
Gladstone, J. C., Copperwheat, C., Heinke, C. O., et al. 2013, ApJS, 206, 14
Godet, O., Lombardi, J. C., Antonini, F., et al. 2014, ApJ, 793, 105
Harrison, F. A., Craig, W. W., Christensen, F. E., et al. 2013, ApJ, 770, 103
Heida, M., Jonker, P. G., Torres, M. A. P., et al. 2014, MNRAS, 442, 1054
Heida, M., Jonker, P. G., Torres, M. A. P., et al. 2016, MNRAS, 459, 771
Heida, M., Torres, M. A. P., Jonker, P. G., et al. 2015, MNRAS, 453, 3511
Israel, G. L., Belfiore, A., Stella, L., et al. 2017a, Sci, 355, 817
Israel, G. L., Papitto, A., Esposito, P., et al. 2017b, MNRAS, 466, L48
Jansen, F., Lumb, D., Altieri, B., et al. 2001, A&A, 365, L1
Kaaret, P., Feng, H., & Gorski, M. 2009, ApJ, 692, 653
Kalberla, P. M. W., Burton, W. B., Hartmann, D., et al. 2005, A&A, 440, 775
Karachentsev, I. D., Dolphin, A. E., Geisler, D., et al. 2002, A&A, 383, 125
King, A., Lasota, J.-P., & Kluźniak, W. 2017, MNRAS, 468, L59
Koliopanos, F., Vasilopoulos, G., Godet, O., et al. 2017, A&A, 608, A47
Lamb, F. K., Pethick, C. J., & Pines, D. 1973, ApJ, 184, 271
Laycock, S. G. T., Maccarone, T. J., & Christodoulou, D. M. 2015, MNRAS, 452, L31
Liu, J.-F., Bregman, J. N., Bai, Y., Justham, S., & Crowther, P. 2013, Nat, 503, 500
López, K. M., Heida, M., Jonker, P. G., et al. 2017, MNRAS, 469, 671
Luangtip, W., Roberts, T. P., & Done, C. 2016, MNRAS, 460, 4417
Méndez, B., Davis, M., Moustakas, J., et al. 2002, AJ, 124, 213
Middleton, M., & King, A. 2017, MNRAS, 470, 69
Middleton, M. J., Heil, L., Pintore, F., Walton, D. J., & Roberts, T. P. 2015, MNRAS, 447, 3243
Miller, J. M., Bachetti, M., Barret, D., et al. 2014, ApJ, 785, L7
Miller, J. M., Walton, D. J., King, A. L., et al. 2013, ApJ, 776, L36
Mitsuda, K., Bautz, M., Inoue, H., et al. 2007, PASJ, 59, 1
Motch, C., Pakull, M. W., Soria, R., Grisé, F., & Pietrzyński, G. 2014, Nat, 514, 198
Mukherjee, E. S., Walton, D. J., Bachetti, M., et al. 2015, ApJ, 808, 64
Mushtukov, A. A., Suleimanov, V. F., Tsygankov, S. S., & Ingram, A. 2017, MNRAS, 467, 1202
Paturel, G., Theureau, G., Fouqué, P., et al. 2002, A&A, 383, 398
Pietrzyński, G., Gieren, W., Hamuy, M., et al. 2010, AJ, 140, 1475
Pinto, C., Alston, W., Soria, R., et al. 2017, MNRAS, 468, 2865
Pinto, C., Middleton, M. J., & Fabian, A. C. 2016, Nat, 533, 64
Pintore, F., Zampieri, L., Stella, L., et al. 2017, ApJ, 836, 113
Poutanen, J., Lipunova, G., Fabrika, S., Butkevich, A. G., & Abolmasov, P. 2007, MNRAS, 377, 1187
Rana, V., Harrison, F. A., Bachetti, M., et al. 2015, ApJ, 799, 121
Ransom, S. M., Eikenberry, S. S., & Middleditch, J. 2002, AJ, 124, 1788
Saha, A., Claver, J., & Hoessel, J. G. 2002, AJ, 124, 839
Servillat, M., Farrell, S. A., Lin, D., et al. 2011, ApJ, 743, 6
Shakura, N. I., & Sunyaev, R. A. 1973, A&A, 24, 337

Soria, R., & Kong, A. 2016, MNRAS, 456, 1837
Soria, R., Musaeva, A., Wu, K., et al. 2017, MNRAS, 469, 886
Steiner, J. F., Narayan, R., McClintock, J. E., & Ebisawa, K. 2009, PASP, 121, 1279
Strüder, L., Briel, U., Dennerl, K., et al. 2001, A&A, 365, L18
Sutton, A. D., Roberts, T. P., Gladstone, J. C., et al. 2013a, MNRAS, 434, 1702
Sutton, A. D., Roberts, T. P., & Middleton, M. J. 2013b, MNRAS, 435, 1758
Sutton, A. D., Roberts, T. P., Walton, D. J., Gladstone, J. C., & Scott, A. E. 2012, MNRAS, 423, 1154
Swartz, D. A., Ghosh, K. K., Tennant, A. F., & Wu, K. 2004, ApJS, 154, 519
Tully, R. B., Courtois, H. M., & Sorce, J. G. 2016, AJ, 152, 50
Verner, D. A., Ferland, G. J., Korista, K. T., & Yakovlev, D. G. 1996, ApJ, 465, 487
Walton, D. J., Fuerst, F., Harrison, F., et al. 2013, ApJ, 779, 148
Walton, D. J., Fürst, F., Harrison, F. A., et al. 2017, ApJ, 839, 105
Walton, D. J., Fürst, F., Harrison, F. A., et al. 2018, MNRAS, 473, 4360
Walton, D. J., Harrison, F. A., Bachetti, M., et al. 2015a, ApJ, 799, 122
Walton, D. J., Harrison, F. A., Grefenstette, B. W., et al. 2014, ApJ, 793, 21
Walton, D. J., Middleton, M. J., Pinto, C., et al. 2016, ApJ, 826, L26
Walton, D. J., Middleton, M. J., Rana, V., et al. 2015b, ApJ, 806, 65
Walton, D. J., Roberts, T. P., Mateos, S., & Heard, V. 2011, MNRAS, 416, 1844
Webb, N., Cseh, D., Lenc, E., et al. 2012, Sci, 337, 554
Wiktorowicz, G., Sobolewska, M., Lasota, J.-P., & Belczynski, K. 2017, ApJ, 846, 17
Wilms, J., Allen, A., & McCray, R. 2000, ApJ, 542, 914